

## Coherent Microwave-to-Optical Conversion via Six-Wave Mixing in Rydberg Atoms

Jingshan Han,<sup>1</sup> Thibault Vogt,<sup>1,2</sup> Christian Gross,<sup>1</sup> Dieter Jaksch,<sup>3,1</sup> Martin Kiffner,<sup>1,3</sup> and Wenhui Li<sup>1,4,\*</sup>  
<sup>1</sup>Centre for Quantum Technologies, National University of Singapore, 3 Science Drive 2, Singapore 117543, Singapore  
<sup>2</sup>MajuLab, CNRS-UNS-NUS-NTU International Joint Research Unit UMI 3654, Singapore 117543, Singapore  
<sup>3</sup>Clarendon Laboratory, University of Oxford, Parks Road, Oxford OX1 3PU, United Kingdom  
<sup>4</sup>Department of Physics, National University of Singapore, Singapore 117542, Singapore

 (Received 31 March 2017; revised manuscript received 18 November 2017; published 1 March 2018)

We present an experimental demonstration of converting a microwave field to an optical field via frequency mixing in a cloud of cold <sup>87</sup>Rb atoms, where the microwave field strongly couples to an electric dipole transition between Rydberg states. We show that the conversion allows the phase information of the microwave field to be coherently transferred to the optical field. With the current energy level scheme and experimental geometry, we achieve a photon-conversion efficiency of  $\sim 0.3\%$  at low microwave intensities and a broad conversion bandwidth of more than 4 MHz. Theoretical simulations agree well with the experimental data, and they indicate that near-unit efficiency is possible in future experiments.

DOI: [10.1103/PhysRevLett.120.093201](https://doi.org/10.1103/PhysRevLett.120.093201)

Coherent and efficient conversion from microwave and terahertz radiation into optical fields and vice versa has tremendous potential for developing next-generation classical and quantum technologies. For example, these methods would facilitate the detection and imaging of millimeter waves with various applications in medicine, security screening, and avionics [1–4]. In the quantum domain, coherent microwave-optical conversion is essential for realizing quantum hybrid systems [5], where spin systems or superconducting qubits are coupled to optical photons that can be transported with low noise in optical fibers [6]. The challenge in microwave-optical conversion is to devise a suitable platform that couples strongly to both frequency bands, which are separated by several orders of magnitude in frequency, and provides an efficient link between them. Experimental work on microwave-optical conversion has been based on ferromagnetic magnons [7], frequency mixing in  $\Lambda$ -type atomic ensembles [8–11], whispering-gallery resonators [12,13], or nanomechanical oscillators [14–16]. All of these schemes include cavities to enhance the coupling to microwaves. The realization of near-unit conversion efficiencies as, e.g., required for transmitting quantum information remains an outstanding and important goal. Recently, highly excited Rydberg atoms have been identified as a promising alternative [17,18], as they feature strong electric dipole transitions in a wide frequency range from microwaves to terahertz [19].

In this Letter, we demonstrate coherent microwave-to-optical conversion of classical fields via six-wave mixing in Rydberg atoms. Because of the strong coupling of millimeter waves to Rydberg transitions, the conversion is realized in free space. In contrast to millimeter-wave induced optical fluorescence [20], frequency mixing is employed here to convert a microwave field into a

unidirectional single frequency optical field. The long lifetime of Rydberg states allows us to make use of electromagnetically induced transparency (EIT) [21], which significantly enhances the conversion efficiency [22]. A free-space photon-conversion efficiency of 0.3% with a bandwidth of more than 4 MHz is achieved with our current experimental geometry. Optimized geometry and energy level configurations should enable the broadband interconversion of microwave and optical fields with near-unit efficiency [17]. Our results, thus, constitute a major step towards using Rydberg atoms for transferring quantum states between optical and microwave photons.

The energy levels for the six-wave mixing are shown in Fig. 1(a), and the experimental setup is illustrated in Fig. 1(b). The conversion of the input microwave field  $M$  into the optical field  $L$  is achieved via frequency mixing with four input auxiliary fields  $P$ ,  $C$ ,  $A$ , and  $R$  in a cold atomic cloud. Starting from the spin polarized ground state  $|1\rangle$ , the auxiliary fields and the microwave field  $M$ , all of which are nearly resonant with the corresponding atomic transitions, create a coherence between the states  $|1\rangle$  and  $|6\rangle$ . This induces the emission of the light field  $L$  with frequency  $\omega_L = \omega_P + \omega_C - \omega_A + \omega_M - \omega_R$  such that the resonant six-wave mixing loop is completed, where  $\omega_X$  is the frequency of field  $X$  ( $X \in \{P, R, M, C, L, A\}$ ). The emission direction of field  $L$  is determined by the phase matching condition  $\mathbf{k}_L = \mathbf{k}_P + \mathbf{k}_C - \mathbf{k}_A + \mathbf{k}_M - \mathbf{k}_R$ , where  $\mathbf{k}_X$  is the wave vector of the corresponding field. The wave vectors of the microwave fields  $\mathbf{k}_A$  and  $\mathbf{k}_M$  are negligible, since they are much smaller than those of the optical fields and, to an excellent approximation, they cancel each other. Moreover, we have  $\mathbf{k}_C \approx \mathbf{k}_R$ , thus the converted light field  $L$  propagates in the same direction as the input field  $P$ . The transverse profile of the converted

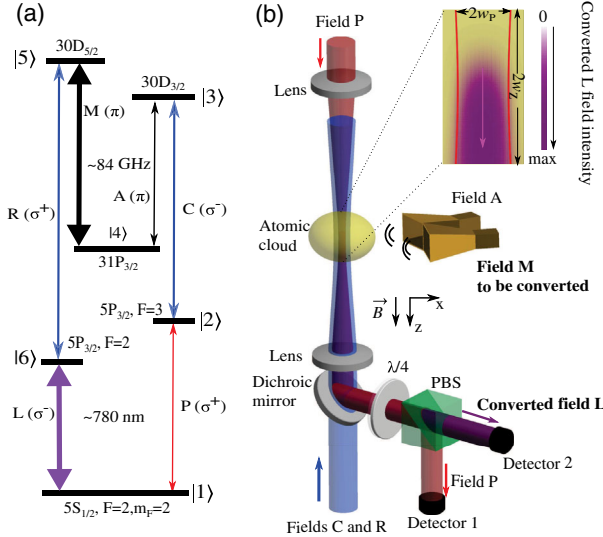


FIG. 1. (a) Relevant energy levels of a  $^{87}\text{Rb}$  atom coupled by six nearly-resonant electromagnetic fields:  $|1\rangle = |5S_{1/2}, F=2, m_F=2\rangle$ ,  $|2\rangle = |5P_{3/2}, F=3, m_F=3\rangle$ ,  $|3\rangle = |30D_{3/2}, m_J=1/2\rangle$ ,  $|4\rangle = |31P_{3/2}, m_J=1/2\rangle$ ,  $|5\rangle = |30D_{5/2}, m_J=1/2\rangle$ , and  $|6\rangle = |5P_{3/2}, F=2, m_F=1\rangle$ . Polarizations of the fields are indicated in brackets. The microwave field  $M$  ( $\approx 84$  GHz) is converted to the light field  $L$  ( $\approx 780$  nm) by six-wave mixing. (b) Experimental setup. Auxiliary light fields  $P$ ,  $C$ , and  $R$  propagate collinearly along the  $z$  axis. They are focused onto the center of a Gaussian-distributed atomic cloud. The fields  $M$  and  $A$  are emitted from horn antennas enclosing an angle of  $20^\circ$ , and propagate horizontally. The bias magnetic field  $B$  along  $z$  defines the quantization axis. The copropagating fields  $L$  and  $P$  are separated by a polarization splitter ( $\lambda/4 + \text{PBS}$ ) and detected simultaneously with avalanche photodiodes. The inset shows the simulated intensity and beam profile of the  $L$  field.

light field  $L$  resembles that of the auxiliary field  $P$  due to pulse matching [23,24] as illustrated in Fig. 1(b).

An experimental measurement begins with the preparation of a cold cloud of  $^{87}\text{Rb}$  atoms in the  $|5S_{1/2}, F=2, m_F=2\rangle$  state in a magnetic field of 6.1 G, as described previously in [25]. At this stage, the atomic cloud has a temperature of about  $70 \mu\text{K}$ , a  $1/e^2$  radius of  $w_z = 1.85(10)$  mm along the  $z$  direction and a peak atomic density  $n_0 = 2.1(2) \times 10^{10} \text{ cm}^{-3}$ . We then switch on all of the input laser and microwave fields simultaneously for frequency mixing. The beams for both  $C$  and  $R$  fields are derived from a single 482 nm laser, while that of the  $P$  field comes from a 780 nm laser, and the two lasers are frequency locked to a single high-finesse temperature stabilized Fabry-Perot cavity [25]. The  $1/e^2$  beam radii of these Gaussian fields at the center of the atomic cloud are  $w_P = 25(1) \mu\text{m}$ ,  $w_C = 54(2) \mu\text{m}$ , and  $w_R = 45(1) \mu\text{m}$ , respectively, and their corresponding peak Rabi frequencies are  $\Omega_P^{(0)} = 2\pi \times 1.14(7)$  MHz,  $\Omega_C^{(0)} = 2\pi \times 9.0(5)$  MHz, and  $\Omega_R^{(0)} = 2\pi \times 6.2(3)$  MHz. The two microwave fields  $M$  and  $A$ , with a frequency separation of around 450 MHz,

are generated by two different microwave sources via frequency multiplication. They are emitted from two separate horn antennas and propagate in the horizontal plane through the center of the atomic cloud, as shown in Fig. 1(b). The Rabi frequencies  $\Omega_M$  and  $\Omega_A$  are approximately uniform across the atomic cloud volume that intersects the laser beams. The Rabi frequency of the  $A$  field is  $\Omega_A = 2\pi \times 1.0(1)$  MHz, while the Rabi frequency of the  $M$  field  $\Omega_M$  is varied in different measurements. The details of the microwave Rabi frequency calibrations are presented in [26]. The  $P$  and  $L$  fields that emerge from the atomic cloud are collected by a diffraction-limited optical system [25], and they are separated using a quarter-wave plate and a polarization beam splitter (PBS). Their respective powers are measured with two different avalanche photodiode detectors. Each optical power measurement is an average of the recorded time-dependent signal in the range from 6 to  $16 \mu\text{s}$  after switching on all the fields simultaneously, where the delay ensures the steady state is fully reached.

We experimentally demonstrate the coherent microwave-to-optical conversion via the six-wave mixing process by two measurements. First, we scan the detuning  $\Delta_P$  of the  $P$  field across the atomic resonance and measure the power of the transmitted field  $P$  ( $P_P$ ) and the power of the converted optical field  $L$  ( $P_L$ ) simultaneously. All other input fields are held on resonance. The results of this measurement are shown in Fig. 2(a), where the spectrum of the transmitted field  $P$  (red squares) exhibits a double peak structure.

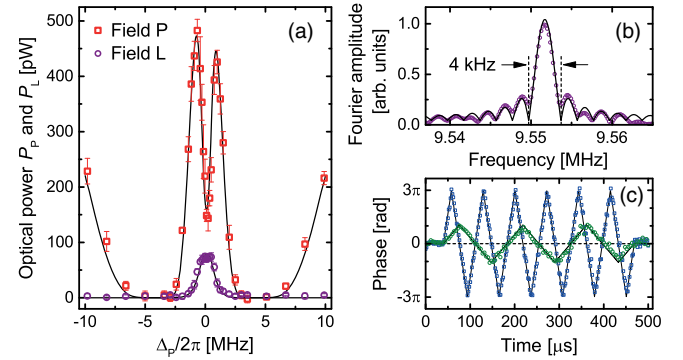


FIG. 2. (a) Spectra of fields  $P$  (red squares) and  $L$  (purple circles). The microwave field  $M$  has detuning  $\Delta_M = 0$  and Rabi frequency  $\Omega_M = 2\pi \times 1.25(12)$  MHz. The error bars indicate the standard deviation of five measurements. The solid curves are obtained from our theoretical model. (b) The Fourier-transformation of the optical heterodyne signal between the  $L$  field and a reference optical field for a pulse duration of  $500 \mu\text{s}$ . The frequency difference between the two fields is  $f_c = 9.5517$  MHz. The solid line shows the fit of a  $|\text{sinc}|$  function to the data. (c) The relative phase of the heterodyne signals for a phase modulated  $M$  field. Triangular modulations of 7 kHz and  $\pi$  amplitude (green circles) and of 14 kHz and  $3\pi$  amplitude (blue squares) are shown. The phase is extracted by numerically demodulating the heterodyne signals [26]. The solid lines show the input phase modulation of the  $M$  field.

The signature of the six-wave mixing process is the converted field  $L$  (purple circles), and its spectrum features a pronounced peak around  $\Delta_P = 0$ .

Second, to verify the coherence of the conversion, we perform optical heterodyne measurements between the  $L$  field and a reference field that is derived from the same laser as the  $P$  field. Figure 2(b) shows that the Fourier spectrum of a 500  $\mu$ s long beat note signal has a transform-limited sinc function dependence. The central frequency of the spectrum confirms that the frequency of the converted field  $L$  is determined by the resonance condition for the six-wave mixing process. Furthermore, we phase modulate the  $M$  field with a triangular modulation function and observe the recovery of the phase modulation in the optical heterodyne measurements, as shown in Fig. 2(c). This demonstrates that the phase information is coherently transferred in the conversion, as expected for a nonlinear frequency mixing process.

We simulate the experimental spectra by modeling the interaction of the laser and microwave fields with the atomic ensemble within the framework of coupled Maxwell-Bloch equations [26]. The time evolution of the atomic density operator  $\rho$  is given by a Markovian master equation ( $\hbar$  is the reduced Planck constant),

$$\partial_t \rho = -\frac{i}{\hbar}[H, \rho] + \mathcal{L}_\gamma \rho + \mathcal{L}_{\text{deph}} \rho, \quad (1)$$

where  $H$  is the Hamiltonian describing the interaction of an independent atom with the six fields, and the term  $\mathcal{L}_\gamma \rho$  describes the spontaneous decay of the excited states. The last term,  $\mathcal{L}_{\text{deph}} \rho$  in Eq. (1), accounts for dephasing of atomic coherences involving the Rydberg states  $|3\rangle$ ,  $|4\rangle$ , and  $|5\rangle$  with the dephasing rates  $\gamma_d$ ,  $\gamma_{DD}$ , and  $\gamma_{d'}$ , respectively [26]. The sources of decoherence are the finite laser linewidths, atomic collisions, and dipole-dipole interactions between Rydberg atoms. The dephasing rates affect the  $P$  and  $L$  spectra and are found by fitting the steady state solution of coupled Maxwell-Bloch equations to the experimental spectra in Fig. 2(a). All other parameters are taken from independent experimental measurements and calibrations. We obtain  $\gamma_d = 2\pi \times 150$  kHz,  $\gamma_{DD} = 2\pi \times 150$  kHz and  $\gamma_{d'} = 2\pi \times 560$  kHz and keep these values fixed in all simulations.

The system in Eq. (1) exhibits an approximate dark state [26],

$$|D\rangle \propto (\Omega_M^* \Omega_C^* |1\rangle - \Omega_M^* \Omega_P |3\rangle + \Omega_A^* \Omega_P |5\rangle), \quad (2)$$

for  $\Omega_L/\Omega_P = -\Omega_A^* \Omega_R^*/(\Omega_M^* \Omega_C^*)$ , where  $\Omega_L$  is the Rabi frequency of field  $L$ . This state has a nonzero population only in metastable states  $|1\rangle$ ,  $|3\rangle$ , and  $|5\rangle$ , and it is decoupled from all of the fields. The population in  $|D\rangle$  increases with the buildup of the converted light field along the  $z$  direction, and thus,  $P_L$  saturates when all atoms are trapped in this state. Figure 3 shows the dependence of the output power  $P_L$  on the optical depth  $D_P \propto n_0 w_z$  of the

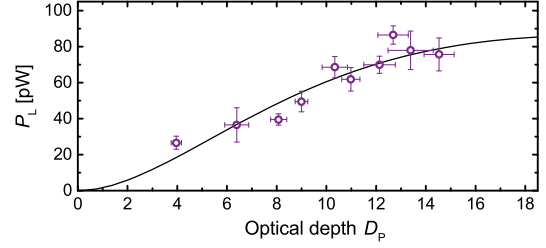


FIG. 3.  $P_L$  vs optical depth  $D_P$ , with all fields on resonance.  $D_P$  is varied by changing  $n_0$ , and the other conditions are the same as for Fig. 2(a). The circles are experimental data, and the solid line is the theoretically simulated curve. The error bars correspond to the standard deviation of four measurements.

atomic cloud, and the theory curve agrees well with the experimental data. The predicted saturation at  $D_P \approx 20$  is consistent with the population in  $|D\rangle$  exceeding 99.8% at this optical depth.

Next, we analyze the dependence of the conversion process on detuning and intensity of the microwave field  $M$ . All auxiliary fields are kept on resonance and at constant intensity. Figure 4(a) shows  $P_L$  as a function of the microwave detuning  $\Delta_M$ . We find that the spectrum of the  $L$  field can be approximated by a squared Lorentzian function centered at  $\Delta_M = 0$ , and its full width at half maximum (FWHM) is  $\approx 6$  MHz. The FWHM extracted from microwave spectra at different intensities  $I_M$  [38] is plotted in Fig. 4(b). The FWHM has a finite value  $>4$  MHz in the low intensity limit, and it increases slowly with  $I_M$  due to power broadening. This large bandwidth is one of the distinguishing features of our scheme, and it is

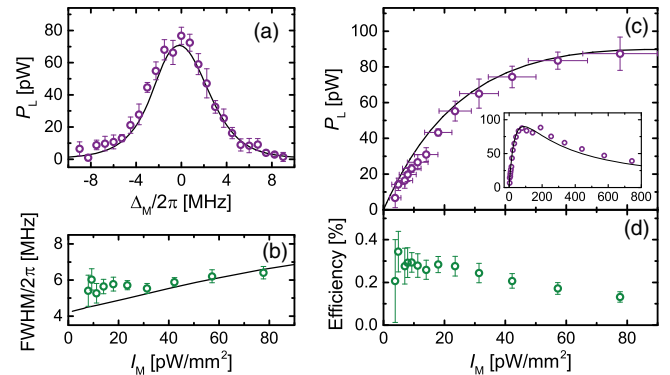


FIG. 4. (a) The spectrum of  $P_L$  against microwave detuning  $\Delta_M$  for  $I_M = 42(8)$  pW/mm $^2$ . (b) FWHM vs  $I_M$ . The FWHM is extracted by fitting a squared Lorentzian function to the spectra. (c)  $P_L$  as a function of  $M$  field intensity  $I_M$ . The inset shows  $P_L$  over a much larger range of  $I_M$ . (d) The efficiency  $\eta$  calculated for the data shown in (c). The circles represent experimental data and solid curves simulation results. The vertical error bars in (a) and (c) correspond to the standard deviation of 4–6 measurements, and in (b) to the errors from fitting. The horizontal error bars in (c) are estimated uncertainties. The error bars in (d) are calculated from those in (c).



essential for extending the conversion scheme to the single-photon level [13]. In Fig. 4(c), we show measurements of  $P_L$  vs the intensity of the microwave field  $I_M$  at  $\Delta_M = 0$ . We find that the converted power  $P_L$  increases approximately linearly at low microwave intensities, and thus, our conversion scheme is expected to work in the limit of very weak input fields. The decrease of  $P_L$  at large intensities arises because the six-wave mixing process becomes inefficient if the Rabi frequency  $\Omega_M$  is much larger than the Rabi frequency  $\Omega_A$  of the auxiliary microwave. All of the theoretical curves in Fig. 4 agree well with the experimental data.

We evaluate the photon-conversion efficiency of our setup by considering the cylindrical volume  $\mathcal{V}$  where the atomic cloud and all six fields overlap. This volume has a diameter  $\sim 2w_P$  and a length  $\sim 2w_z$  [see Fig. 1(b)]. We define the conversion efficiency as

$$\eta = \frac{P_L/\hbar\omega_L}{I_M S_M/\hbar\omega_M}, \quad (3)$$

where  $S_M = 4w_P w_z$  is the cross section of the volume  $\mathcal{V}$  perpendicular to  $\mathbf{k}_M$ . The efficiency  $\eta$  gives the ratio of the photon flux in  $L$  leaving volume  $\mathcal{V}$  over the photon flux in  $M$  entering  $\mathcal{V}$ . As shown in Fig. 4(d), the conversion efficiency is approximately  $\eta \approx 0.3\%$  over a range of low intensities, and then it decreases with increasing  $I_M$ . Note that  $\eta$  in Eq. (3) is a measure of the efficiency of the physical conversion process in the Rydberg medium based on the microwave power  $I_M S_M$  impinging on  $S_M$ . This power is smaller than the total power emitted by the horn antenna since the  $M$  field has not been focused on  $\mathcal{V}$  in our setup.

The good agreement between our model and the experimental data allows us to theoretically explore other geometries. To this end, we consider that the microwave fields  $M$  and  $A$  are copropagating with the  $P$  field, and we assume that all other parameters are the same [26]. We numerically evaluate the generated light power  $P_L^{\parallel}$  for this setup and calculate the efficiency  $\eta^{\parallel}$  by replacing  $P_L$  with  $P_L^{\parallel}$  and  $S_M$  with  $S_M^{\parallel} = \pi w_P^2$  in Eq. (3). We find  $\eta^{\parallel} \approx 26\%$ , which is approximately two orders of magnitude larger than  $\eta$ . This increase is mostly due to the geometrical factor  $S_M/S_M^{\parallel} \approx 91$ , since  $P_L^{\parallel} \sim P_L$ . Note that such a value for  $\eta^{\parallel}$  is consistent with the efficiency achieved by a similar near-resonance frequency mixing scheme in the optical domain [39].

In conclusion, we have demonstrated coherent microwave-to-optical conversion via a six-wave mixing process utilizing the strong coupling of electromagnetic fields to Rydberg atoms. We have established the coherence of the conversion by a heterodyne measurement and demonstrated a large bandwidth by measuring the generated light as a function of the input microwave frequency. Coherence

and large bandwidth are essential for taking our scheme to the single-photon level and using it in quantum technology applications. Our results are in good agreement with theoretical simulations based on an independent-atom model, thus showing a limited impact of atom-atom interactions on our conversion scheme.

This work has focussed on the physical conversion mechanism in Rydberg systems and provides several possibilities for future studies and applications. Alkali-metal-atom transitions offer a wide range of frequencies in the optical and microwave domain with properties similar to those exploited in this work. For example, the conversion of a microwave field to telecommunication wavelengths is possible by switching to different optical transitions and/or using different atomic species [18,40,41], which makes our approach promising for classical and quantum communication applications. Moreover, it has been theoretically shown that bidirectional conversion with near-unit efficiency is possible by using a different Rydberg excitation scheme and well-chosen detunings of the auxiliary fields [17]. Such a nonlinear conversion with near-unit efficiency has only been experimentally realized in the optical domain [42]. Reaching this level of efficiency requires good mode matching between the millimeter waves and the auxiliary optical fields [17], which can be achieved either by tightly focusing the millimeter wave or by confining it to a waveguide directly coupled to the conversion medium [11,43]. Eventually, extending our conversion scheme to millimeter waves in a cryogenic environment [44,45] would pave the way towards quantum applications.

The authors thank Tom Gallagher for useful discussions and acknowledge the support by the National Research Foundation, Prime Minister's office, Singapore and the Ministry of Education, Singapore under the Research Centres of Excellence programme. This work is partly supported by Singapore Ministry of Education Academic Research Fund Tier 2 (Grant No. MOE2015-T2-1-085). M. K. would like to acknowledge the use of the University of Oxford Advanced Research Computing (ARC) facility [46].

---

\* wenhui.li@nus.edu.sg

- [1] A. J. L. Adam, Review of near-field terahertz measurement methods and their applications, *J. Infrared Millim. Waves* **32**, 976 (2011).
- [2] W. L. Chan, J. Deibel, and D. M. Mittleman, Imaging with terahertz radiation, *Rep. Prog. Phys.* **70**, 1325 (2007).
- [3] M. Tonouchi, Cutting-edge terahertz technology, *Nat. Photonics* **1**, 97 (2007).
- [4] X. C. Zhang, A. Shkurinov, and Y. Zhang, Extreme terahertz science, *Nat. Photonics* **11**, 16 (2017).
- [5] Z.-L. Xiang, S. Ashhab, J. Q. You, and F. Nori, Hybrid quantum circuits: Superconducting circuits interacting with other quantum systems, *Rev. Mod. Phys.* **85**, 623 (2013).

- [6] H. J. Kimble, The quantum internet, *Nature (London)* **453**, 1023 (2008).
- [7] R. Hisatomi, A. Osada, Y. Tabuchi, T. Ishikawa, A. Noguchi, R. Yamazaki, K. Usami, and Y. Nakamura, Bidirectional conversion between microwave and light via ferromagnetic magnons, *Phys. Rev. B* **93**, 174427 (2016).
- [8] L. A. Williamson, Y.-H. Chen, and J. J. Longdell, Magneto-Optic Modulator with Unit Quantum Efficiency, *Phys. Rev. Lett.* **113**, 203601 (2014).
- [9] C. O'Brien, N. Lauk, S. Blum, G. Morigi, and M. Fleischhauer, Interfacing Superconducting Qubits and Telecom Photons via a Rare-Earth-Doped Crystal, *Phys. Rev. Lett.* **113**, 063603 (2014).
- [10] S. Blum, C. O'Brien, N. Lauk, P. Bushev, M. Fleischhauer, and G. Morigi, Interfacing microwave qubits and optical photons via spin ensembles, *Phys. Rev. A* **91**, 033834 (2015).
- [11] M. Hafezi, Z. Kim, S. L. Rolston, L. A. Orozco, B. L. Lev, and J. M. Taylor, Atomic interface between microwave and optical photons, *Phys. Rev. A* **85**, 020302 (2012).
- [12] D. V. Strekalov, H. G. L. Schwefel, A. A. Savchenkov, A. B. Matsko, L. J. Wang, and N. Yu, Microwave whispering-gallery resonator for efficient optical up-conversion, *Phys. Rev. A* **80**, 033810 (2009).
- [13] A. Rueda, F. Sedlmeir, M. C. Collodo, U. Vogl, B. Stiller, G. Schunk, D. V. Strekalov, C. Marquardt, J. M. Fink, O. Painter, G. Leuchs, and H. G. L. Schwefel, Efficient microwave to optical photon conversion: An electro-optical realization, *Optica* **3**, 597 (2016).
- [14] J. Bochmann, A. Vainsencher, D. D. Awschalom, and A. N. Cleland, Nanomechanical coupling between microwave and optical photons, *Nat. Phys.* **9**, 712 (2013).
- [15] R. W. Andrews, R. W. Peterson, T. P. Purdy, K. Cicak, R. W. Simmonds, C. A. Regal, and K. W. Lehnert, Bidirectional and efficient conversion between microwave and optical light, *Nat. Phys.* **10**, 321 (2014).
- [16] T. Bagci, A. Simonsen, S. Schmid, L. G. Villanueva, E. Zeuthen, J. Appel, J. M. Taylor, A. Sørensen, K. Usami, A. Schliesser *et al.*, Optical detection of radio waves through a nanomechanical transducer, *Nature (London)* **507**, 81 (2014).
- [17] M. Kiffner, A. Feizpour, K. T. Kaczmarek, D. Jaksch, and J. Nunn, Two-way interconversion of millimeter-wave and optical fields in Rydberg gases, *New J. Phys.* **18**, 093030 (2016).
- [18] B. T. Gard, K. Jacobs, R. McDermott, and M. Saffman, Microwave-to-optical frequency conversion using a cesium atom coupled to a superconducting resonator, *Phys. Rev. A* **96**, 013833 (2017).
- [19] T. F. Gallagher, *Rydberg Atoms* (Cambridge University Press, Cambridge, 1994).
- [20] C. G. Wade, N. Šibalić, N. R. de Melo, J. M. Kondo, C. S. Adams, and K. J. Weatherill, Real-time near-field terahertz imaging with atomic optical fluorescence, *Nat. Photonics* **11**, 40 (2017).
- [21] A. K. Mohapatra, T. R. Jackson, and C. S. Adams, Coherent Optical Detection of Highly Excited Rydberg States Using Electromagnetically Induced Transparency, *Phys. Rev. Lett.* **98**, 113003 (2007).
- [22] M. Fleischhauer, A. Imamoglu, and J. P. Marangos, Electromagnetically induced transparency: Optics in coherent media, *Rev. Mod. Phys.* **77**, 633 (2005).
- [23] S. E. Harris, Electromagnetically Induced Transparency with Matched Pulses, *Phys. Rev. Lett.* **70**, 552 (1993).
- [24] S. E. Harris, Normal Modes for Electromagnetically Transparency, *Phys. Rev. Lett.* **72**, 52 (1994).
- [25] J. Han, T. Vogt, M. Manjappa, R. Guo, M. Kiffner, and W. Li, Lensing effect of electromagnetically induced transparency involving a Rydberg state, *Phys. Rev. A* **92**, 063824 (2015).
- [26] See Supplemental Material at <http://link.aps.org/supplemental/10.1103/PhysRevLett.120.093201>, which also contains Refs. [27–37], for details about the theoretical model and the calibration of experimental parameters.
- [27] J. Han, T. Vogt, and W. Li, Spectral shift and dephasing of electromagnetically induced transparency in an interacting Rydberg gas, *Phys. Rev. A* **94**, 043806 (2016).
- [28] Wolfram Research, Inc., *Mathematica Version 10.1*, Wolfram Research, Inc., Irvine, 2015.
- [29] D. A. Steck, Rubidium 87D Line Data, <http://steck.us/alkalidata> (revision 2.1.4, 23 December 2010).
- [30] I. I. Beterov, I. I. Ryabtsev, D. B. Tretyakov, and V. M. Entin, Quasiclassical calculations of blackbody-radiation-induced depopulation rates and effective lifetimes of Rydberg  $nS$ ,  $nP$ , and  $nD$  alkali-metal atoms with  $n \leq 80$ , *Phys. Rev. A* **79**, 052504 (2009).
- [31] D. B. Branden, T. Juhasz, T. Mahlokozera, C. Vesa, R. O. Wilson, M. Zheng, A. Kortyna, and D. A. Tate, Radiative lifetime measurements of rubidium Rydberg states, *J. Phys. B* **43**, 015002 (2010).
- [32] E. Arimondo, V coherent population trapping in laser spectroscopy, *Prog. Opt.* **35**, 257 (1996).
- [33] M. Tanasittikosol, J. Pritchard, D. Maxwell, A. Gauguier, K. Weatherill, R. Potvliege, and C. Adams, Microwave dressing of Rydberg dark states, *J. Phys. B* **44**, 184020 (2011).
- [34] G. Grynberg, A. Aspect, and C. Fabre, *Introduction to Quantum Optics: From the Semi-Classical Approach to Quantized Light* (Cambridge University Press, Cambridge, 2010).
- [35] J. A. Sedlacek, A. Schwettmann, H. Kübler, R. Löw, T. Pfau, and J. P. Shaffer, Microwave electrometry with Rydberg atoms in a vapour cell using bright atomic resonances, *Nat. Phys.* **8**, 819 (2012).
- [36] C. L. Holloway, J. A. Gordon, A. Schwarzkopf, D. A. Anderson, S. A. Miller, N. Thaicharoen, and G. Raitchel, Sub-wavelength imaging and field mapping via electromagnetically induced transparency and Autler-Townes splitting in Rydberg atoms, *Appl. Phys. Lett.* **104**, 244102 (2014).
- [37] J. A. Gordon, C. L. Holloway, A. Schwarzkopf, D. A. Anderson, S. Miller, N. Thaicharoen, and G. Raitchel, Millimeter wave detection via Autler-Townes splitting in rubidium Rydberg atoms, *Appl. Phys. Lett.* **105**, 024104 (2014).
- [38] The intensity  $I_M$  is related to the Rabi frequency  $\Omega_M$  by  $I_M = \frac{1}{2} \epsilon_0 c (\hbar \Omega_M / d_{45})^2$ , where  $c$  is the speed of the light,  $\epsilon_0$  the electric constant,  $\hbar$  the Planck constant, and  $d_{45}$  is the

- electric dipole moment between states  $|4\rangle$  and  $|5\rangle$  (See Ref. [26]).
- [39] A. J. Merriam, S. J. Sharpe, M. Shverdin, D. Manuszak, G. Y. Yin, and S. E. Harris, Efficient Nonlinear Frequency Conversion in an All-Resonant Double- $\Lambda$  System, *Phys. Rev. Lett.* **84**, 5308 (2000).
- [40] S. L. Gilbert, Frequency stabilization of a fiber laser to rubidium: A high-accuracy  $1.53 - \mu\text{m}$  wavelength standard, *Proc. SPIE Int. Soc. Opt. Eng.* **1837**, 146 (1993).
- [41] M. A. Bouchiat, J. Guéna, P. Jacquier, M. Lintz, and L. Pottier, The  $\text{cs } 6s-7s-6p_{3/2}$  forbidden three-level system: analytical description of the inhibited fluorescence and optical rotation spectra, *J. Phys. (Paris)* **50**, 157 (1989).
- [42] A. J. Merriam, S. J. Sharpe, H. Xia, D. Manuszak, G. Y. Yin, and S. E. Harris, Efficient gas-phase generation of coherent vacuum ultraviolet radiation, *Opt. Lett.* **24**, 625 (1999).
- [43] S. D. Hogan, J. A. Agner, F. Merkt, T. Thiele, S. Filipp, and A. Wallraff, Driving Rydberg-Rydberg Transitions from a Coplanar Microwave Waveguide, *Phys. Rev. Lett.* **108**, 063004 (2012).
- [44] C. Hermann-Avigliano, R. C. Teixeira, T. L. Nguyen, T. Cantat-Moltrecht, G. Nogues, I. Dotsenko, S. Gleyzes, J. M. Raimond, S. Haroche, and M. Brune, Long coherence times for Rydberg qubits on a superconducting atom chip, *Phys. Rev. A* **90**, 040502 (2014).
- [45] D. Cano, H. Hattermann, B. Kasch, C. Zimmermann, R. Kleiner, D. Koelle, and J. Fortágh, Experimental system for research on ultracold atomic gases near superconducting microstructures *Eur. Phys. J. D* **63**, 17 (2011).
- [46] <http://dx.doi.org/10.5281/zenodo.22558>.